Journal of Cleaner Production 418 (2023) 138147

Contents lists available at ScienceDirect

Journal of Cleaner Production

journal homepage: www.elsevier.com/locate/jclepro

# Modeling and thermodynamic optimization of a solar-driven two-stage multi-element thermoelectric generator

Congzheng Qi [a,b,c,1], Yuxuan Du [a,b,d,1], Lingen Chen [a,b,c,*], Yong Yin [a,b,d], Yanlin Ge [a,b,c]

[a] Institute of Thermal Science and Power Engineering, Wuhan Institute of Technology, Wuhan, 430205, China
[b] Hubei Provincial Engineering Technology Research Center of Green Chemical Equipment, Wuhan, 430205, China
[c] School of Mechanical & Electrical Engineering, Wuhan Institute of Technology, Wuhan, 430205, China
[d] School of Optical Information and Energy Engineering, Wuhan Institute of Technology, Wuhan, 430205, China

ARTICLE INFO

Handling Editor: Jin-Kuk Kim

*Keywords:*
Finite-time thermodynamics
Solar-driven thermoelectric device
Two-stage thermoelectric generator
Optimal performance
Power
Efficiency

ABSTRACT

In this article, a finite-time thermodynamic model of solar-driven two-stage multi-element thermoelectric generator is developed. Considering external heat transfers, radiation loss of collector, Joule heat and Fourier heat leakage, analytical formulas for heat balance equations, power and efficiency are derived. Working temperatures of thermoelectric device are obtained by solving four equations simultaneously, and basic performance of the system is explored. Performance optimization is executed by adjusting electrical current, thermoelectric element distribution and heat exchanger inventory distribution. The optimal allocations for different total thermoelectric element numbers are given by the enumeration method. Influences of various factors on maximal power and efficiency are analyzed, and the upper bounds of power and efficiency are given. Results show that an optimal collector temperature exists to achieve optimal performance for this solar power device. Power and efficiency show the same variation trend, and the efficiency is maximal when power reaches its maximum. The system performance is optimal when external heat transfers and inner structure parameters are optimal. At this time, the corresponding junction temperatures reach their optimal values, the total thermal conductance should be divided in a half to two heat exchangers, and the corresponding thermoelectric element is allocated nearly half to upper generator.

## 1. Introduction

Thermoelectric generator (TEG) is a new power generating system that can convert heat to electrical current directly by using thermoelectric couple as working element. Unlike traditional cylindrical rotating generators, TEG devices are simple in structure and have no moving parts. Therefore, they have the characteristics of stability, silence and long life in operation. With the improvement of TEG efficiency and reduction of the manufacturing cost of semiconductor materials, TEG has been widely applied in military, medical, satellite vehicles and other fields (He et al., 2015; Tohidi et al., 2022). At present, there are two main directions in the research of thermoelectric devices. On the one hand, it focuses on the discovery and improvement of new thermoelectric materials, which belongs to the category of materials science (Patil et al., 2018); on another hand, is to study the thermodynamic performance based on different TEG devices, so that the improvement of structure and energy conversion efficiency can be guided (Shittu et al., 2020). This paper will study TEG devices from the second aspect, and propose a new architecture for TEG device further.

In the early stage, the performance analyses of thermoelectric devices were mainly carried out by non-equilibrium thermodynamics (NET). The heat-reservoir temperatures were generally regarded as the junction temperatures of TEG when explored the heat flow conversion, and the external heat resistances were ignored. For example, Ranjbar et al. (2021) studied a hybrid device performance consisting of a thermionic generator and TEG. Cai et al. (2023) established a TEG model driven by hot exhaust gas from truck exhaust pipes, and obtained maximal power by optimizing the size of thermoelectric element. Some scholars have also studied the performance of TEG devices with ANSYS software. Aranguren et al. (2017) proposed a TEG device placed on high chimney walls for waste heat recovery, and investigated the relation between flue gas temperature loss and power generation performance. Selimefendigil and Öztop (2020) established a TEG model mounted

* Corresponding author. Institute of Thermal Science and Power Engineering, Wuhan Institute of Technology, Wuhan, 430205, China.
*E-mail addresses:* lingenchen@hotmail.com, 2506715339@qq.com (L. Chen).
[1] The two authors have the same contribution.

https://doi.org/10.1016/j.jclepro.2023.138147
Received 14 June 2023; Received in revised form 10 July 2023; Accepted 16 July 2023
Available online 17 July 2023
0959-6526/© 2023 Elsevier Ltd. All rights reserved.

**Nomenclature**

| | |
|---|---|
| $A$ | Area of receiver, $m^2$ $C$ Concentration ratio |
| $G$ | Solar insolation, $W/m^2$ $I$ Electrical current, $AK$ Thermal conductance, $W/KK_T$ Total heat exchanger inventory, $W/KM$ Total thermoelectric element number |
| $m$ | Thermoelectric element number of upper thermoelectric generator |
| $n$ | Thermoelectric element number of bottom thermoelectric generator |
| $P$ | Output power, $WQ$ Heat flux, $WR$ Electrical resistance, $\Omega T$ Temperature, $Kx$ Heat exchanger inventory ratio |

*Greek symbols*

| | |
|---|---|
| $\alpha$ | Seebeck coefficient, $V/K$ |
| $\sigma$ | Stefan-Boltzmann constant, $W/(m^2 \cdot K^4)$ |
| $\varepsilon$ | Emissivity of receiver |
| $\eta_{op}$ | Optical efficiency of concentrator |
| $\eta$ | Efficiency of system |
| $\Delta T$ | Temperature difference, $K$ |

*Abbreviations*

| | |
|---|---|
| FTT | NET Finite-time thermodynamics Non-equilibrium thermodynamics |
| TEG | Thermoelectric generator |
| TER | Thermoelectric refrigerator |
| TEHP | Thermoelectric heat pump |

between two water channels with rotating cylinders, and studied the effects of the size and number of rotating cylinders on power. Chen et al. (2022a) built a TEG model coupled with square vehicle exhaust channels, and studied the effects of leg height on thermal stress and output power. They established 3D models to study the internal heat transfers of thermoelectric modules or the effects of fluid flow in external channels, so as to improve system performances. However, these efforts focused on optimizing the geometry dimension of thermoelectric modules, but neglected the study of external heat transfers. Therefore, these works belonged to the research content of NET from thermodynamics and heat transfer standpoints. Meanwhile, Refs (Mirhosseini et al., 2019; Karana and Sahoo, 2021; Ebrahimi et al., 2022; Yuan et al., 2023). also performed NET analyses and optimizations for various single-stage TEGs.

In fact, TEG can't generate electricity independently, it must connect with heat exchangers to gain and dissipate heat, so the external heat resistance shouldn't be neglected. Although the reservoir temperatures are fixed, the junction temperatures of TEG are dynamic under different working conditions due to external heat resistances. In addition, NET lacks the optimization for external heat transfer processes, and it can't reflect the actual change law of energy conversion processes. Therefore, these research methods have obvious limitations.

Finite-time thermodynamics (FTT) (Curzon and Ahlborn, 1975; Andresen, 1983, 2011; Chen et al., 1999, 2016; Pourkiaei et al., 2019; Berry et al., 2020; Sieniutycz, 2020; Andresen and Salamon, 2022) is a tremendous advance for modern thermodynamics, and it stems from the pioneering work of Curzon and Ahlborn (1975) on endoreversible Carnot engine in 1975. FTT provides a method to investigate the external heat transfer irreversibilities, it takes the system with finite-rate heat transfer processes between device and reservoir as research object, and optimizes system performance under the constraints of finite time and size, which can well solve the problems existing in NET. Therefore, the performance limits obtained by FTT can provide more reasonable guidance for actual thermoelectric devices. Since the foundational paper of Curzon and Ahlborn was published, a lot of works have been executed about different thermal, chemical and electrical processes and devices, such as finite-reservoir heat-pump (Chen and Xia, 2023a) and heat-engine (Chen and Xia, 2022a, 2023b; Li and Chen, 2022) cycles, organic-Rankine-cycles (Wu et al., 2020, 2021a; Feng et al., 2021; Yang et al., 2023), internal-combustion-cycles (Ge et al., 2021, 2022a, 2022b, 2023; Wu et al., 2021b; Zang et al., 2022; Chen et al., 2023a), Stirling cooler (Paul and Hoffmann, 2022; Prajapati et al., 2023) and heat-engine (Xu et al., 2022) cycles, thermal-Brownian-cycles (Qi et al., 2021; Chen et al., 2022b), blue-engine-cycle (Lin et al., 2022), thermoradiative-devices (Hu et al., 2021; Zhang et al., 2021), thermionic-devices (Qiu et al., 2021a; Liang et al., 2022), electron-engine (Qiu et al., 2021b), membrane-reactors (Li et al., 2022a, 2022b; Kong et al., 2022; Chen et al., 2022c), chemical-engine-cycles (Chen and Xia, 2022b, 2022c, 2023c, 2023d, 2023e), chemical-pump cycles (Chen et al., 2020a, 2023b, 2023c, 2023d), etc. These related researches enrich the application range of FTT, and the results obtained are more reliable.

At present, many related pieces of research on TEG have been performed by applying FTT (Chen et al., 2016; Pourkiaei et al., 2019). Gordon (1991) considered external finite-rate heat transfers, and optimized single-element TEG performance firstly. However, commercial TEG devices are usually composed of multiple semiconductor elements. Subsequently, the performances of multi-element TEG devices were also studied. Chen et al. (2002) studied multi-element TEG performance under Newtonian heat transfer law, and analyzed the thermoelectric element number effect on optimal performance. The external heat transfers have many forms, and they affect the device performance strongly. Based on the multi-element TEG model, Chen and his colleges (Chen et al., 2005a, 2012; Meng et al., 2012) compared the performance differences when external heat transfer followed linear phenomenological law (Chen et al., 2005a), radiative law (Meng et al., 2012), as well as generalized law (Chen et al., 2012), respectively. The optimal electrical currents and thermal conductance allocations for maximal power were also given. To reach a compromise between power and efficiency, Tian et al. (2022a) studied the multi-element TEG performance under efficient power criteria. Unfortunately, the underutilized heat is dissipated into environment directly for above TEG devices, which means the wastage of energy.

The multi-stage thermal device can recycle heat in different grades, and the energy utilization was improved due to the enlargement of operating temperature difference when the TEG worked in tandem. Subsequently, a FTT model of two-stage TEG device was developed by Chen et al. (2005b) firstly, and the performance was optimized by modulating heat exchanger area allocation and thermoelectric element number allocation. Based on this model, Tian et al. (2022b) performed a multi-objective optimization by NSGA-II algorithm further. The above scholars explored the optimal performance of TEG devices from single-element to multi-element structure, and from single-stage to two-stage structure.

Some scholars have also carried out research on thermoelectric refrigerator (TER), thermoelectric heat-pump (TEHP), as well as their combined devices. Chen and his colleges (Chen et al., 2021; Chen and Lorenzini, 2022) compared the performance difference of multi-element TER when the heat transfer followed Newtonian law, linear phenomenological law and radiative law, respectively. Chen et al. (2020b) and Jiang et al. (2022) proposed an air-cooled and a water-cooled TER model, respectively. The influences of radiator performance and module packing factor on cooling load were also studied. Ma et al. (2023) applied TER device to improve the building environment, and realized the effective regulation of indoor temperature. Recently, some scholars proposed some combined thermoelectric devices, such as the single-stage TEG-TER device (Feng et al., 2018), single-stage TEG-TEHP device (Chen and Lorenzini, 2023) and two-stage TEG-TEHP device (Chen et al., 2020c), and obtained a lot of interesting results for the design of actual devices, see the comprehensive reviews (Chen et al., 2016; Pourkiaei et al., 2019).

Different from traditional shaft generator devices, the TEG can work stably without any external mechanical work, and it has a lower requirement for heat-reservoir grade. Benefiting from this feature, the TEG can generate electricity with the help of different kinds of heat reservoirs. When the fuel cell offered electricity for external devices, a vast amount of waste heat was also dissipated into environment. Zhang et al. (2017) proposed a combined device that employed a two-stage TEG to reuse the waste heat of fuel cells. Guo et al. (2020) further optimized the hybrid device performance consisting of fuel cells and two-stage TEG with Thomson effect. Meng et al. (2017) established a water-cooled TEG model for recycling industrial gas waste heat, and studied the relation between the gas inlet temperature and the optimal thermoelectric element length. Xiong et al. (2014) built a TEG model for recycling waste heat from slag water, and optimized the inner structural parameters for maximum power. Xiong et al. (2016) built a two-stage cylindrical TEG model driven by sintering flue gas, and studied the invest recovery period. Ghoreishi et al. (2023) optimized the external hot fluid channel geometrical parameters of waste heat recovery TEG device. Zhao et al. (2023) found that the power could be improved rapidly by inserting a perforated plate in external heat exchangers. Cheng et al. (2018) designed multi-stage TEG devices to reuse the combustion heat of hypersonic vehicle, and analyzed maximal efficiency under large temperature difference conditions. Zhu et al. (2022) proposed an annular TEG device attached to the surface of a pipe with internal twisted tape, and studied the effects of twist ratio of twisted tape on power generation performance. The above researches achieved power generation by using different types of waste heat, and improved the energy utilization efficiency effectively.

Solar energy is a kind of completely green energy, and it has a rich reserve and wide distribution. With the advancement of solar collector technology (Xiong et al., 2021), the combination of solar collector systems and TEG systems attracts the interest of numerous researchers from all over the world. Recently, some scholars have studied the performance of solar TEG devices by using NET. Tayebi et al. (2014) studied solar single-element TEG operated in a vacuum thin-film package, and the research showed that the thin-film structure could enhance solar energy utilization effectively. Bellos and Tzivanidis (2020) investigated the performance of a solar single-element TEG without concentrator, and gave the maximal efficiency. Meanwhile, some scholars also carried out research on the solar multi-element TEG devices. Suter et al. (2011) proposed a multi-element solar TEG device arranged on the hollow cube surface, and studied the influence of cavity size on output power. Sun et al. (2022) proposed a multi-element solar TEG model to predict the power generation performance during whole daytime through a 3D transient numerical model. Montero et al. (2021) proposed a solar multi-element TEG model with a heat storage unit, and results showed that the solar TEG performance could be improved by this unit. Musharavati et al. (2022) proposed a hybrid model of TEG driven by waste heat of solar salinity energy storage pond, and gave its maximal net power. These solar device models (Tayebi et al., 2014; Bellos and Tzivanidis, 2020; Suter et al., 2011; Sun et al., 2022; Montero et al., 2021; Musharavati et al., 2022) ignored the external heat resistances, and the external heat transfer processes were not optimized in deriving optimal performances.

Some scholars also studied the solar TEG device performance by FTT, Chen (1996) proposed a FTT model for solar-driven single-element TEG firstly, and optimized its efficiency by optimizing electrical current. To realize the cascade utilization of energy, Eke et al. (2022) built a FTT model for solar-driven two-stage TEG device consisting of two single-element TEGs, and gave the maximal efficiency by optimizing the geometries of thermoelectric leg and load resistance with ANSYS software. Although the external heat resistances were considered in this model, the optimization for heat transfer processes was neglected. Therefore, the maximal efficiency couldn't represent the actual limit. Meanwhile, many relevant experiments have been carried out in recent years for actual performance. However, these studies mainly focused on solar single-stage TEG devices (Tyagi et al., 2023). Lv et al. (2019) carried out an experimental study on a heat pipe solar TEG device, and the effects of solar insolation, solar collector performance and ambient temperature on efficiency were studied. Subsequently, they further investigated solar TEG device performance under realistic fluctuating radiation (Lv et al., 2021), and found that power generation performance was best at noon.

Based on above literature survey, the solar TEG has important application value in alleviating the energy crisis. Since the current FTT model of solar two-stage TEG has a single-element structure (Eke et al., 2022), while the practical devices are usually multi-element structure, so this model needs to be improved. In addition, an overall performance optimization was also not provided in previous works. To fill this research gap, this paper will develop a solar-driven two-stage TEG model with a multi-element structure. Considering the multi-irreversibilities existing in practice, the power, efficiency and heat balance equations of the new model will be deduced by FTT and NET. The receiver and junction temperatures will be solved by simultaneous equations, and the performance characteristics of new device will be studied and optimized by adjusting internal structural parameters and external heat transfer processes. Influences of ambient temperature, total inventory and solar insolation on optimal performance will also be studied. The solar two-stage TEG in this paper can be used to improve the energy utilization efficiency for actual solar thermoelectric devices. The performance limits derived can also provide theoretical guidance for the performance optimization of practical solar TEG systems.

## 2. Model and heat flow analysis

Fig. 1 gives a solar-driven two-stage TEG diagram. The device is composed of a solar thermal collector, two-stage TEG and heat exchangers. The collector converts solar radiation into heat, it consists of two parts: concentrator and receiver, and the receiver temperature is $T_H$.

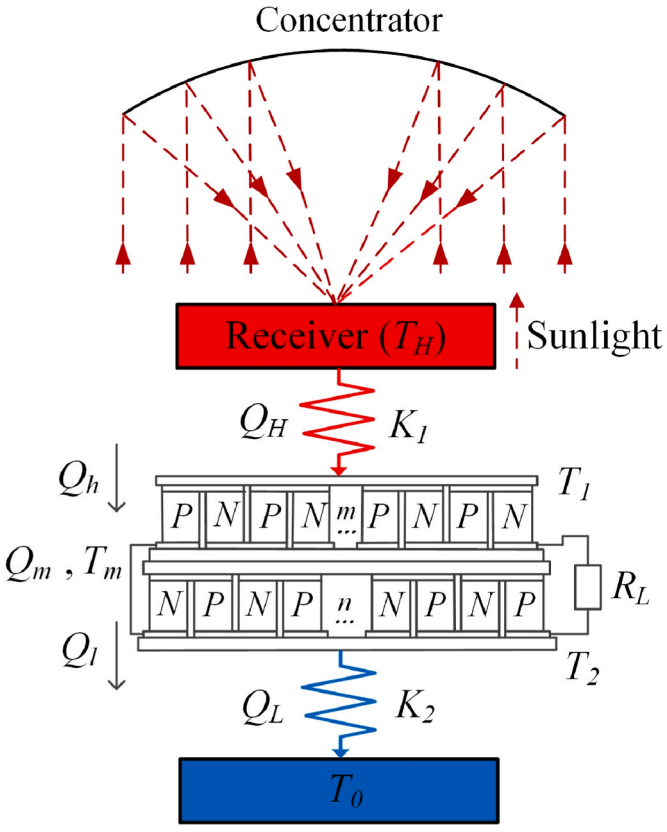


**Fig. 1.** Solar-driven two-stage multi-element TEG device.

The TEG gets heat from receiver through upper heat exchanger, the two junction temperatures are $T_1$ and $T_2$, and the connection layer temperature is $T_m$. The upper (or bottom) TEG contains $m$ (or $n$) pairs of thermoelectric elements, the total number is $M$ ($M = m + n$), and both $m$ and $n$ are integers. The waste heat is discharged to environment through the bottom heat exchanger, and ambient temperature is $T_0$, one has $T_H > T_1 > T_m > T_2 > T_0$. The heat flux between receiver (or environment) and TEG is $Q_H$ (or $Q_L$). $K_1$ and $K_2$ are thermal conductance, and overall inventory is $K_T$ ($K_T = K_1 + K_2$). $K$ is the total thermal conductance of thermoelectric couple. The heat fluxes of three junctions are $Q_h$, $Q_l$ and $Q_m$, and $R_L$ is external electrical resistance.

The solar collector converts solar energy into heat, some of which is dissipated into environment in the form of radiation, and the rest is used to heat TEG. When the sunlight intensity remains stationary, the heat utilizable for TEG per unit time can be expressed as (Lai et al., 2019; Qiu et al., 2022):

$$Q_H = CGA\eta_{op} - \varepsilon\sigma A\left(T_H^4 - {T_0}^4\right) \tag{1}$$

where $C$ is concentration ratio, $G$ is solar insolation, $A$ is collector area, $\eta_{op}$ is optical efficiency of concentrator, $\varepsilon$ is emissivity of receiver, and $\sigma$ is Stefan-Boltzmann constant.

For two-stage TEG, the heat fluxes $Q_h$, $Q_m$ and $Q_l$ at three junctions are:

$$Q_h = m\left[\alpha I T_1 - I^2R/2 + K(T_1 - T_m)\right] \tag{2}$$

$$Q_m = m\left[\alpha I T_m + I^2R/2 + K(T_1 - T_m)\right] \tag{3}$$

$$Q_m = n\left[\alpha I T_m - I^2R/2 + K(T_m - T_2)\right] \tag{4}$$

$$Q_l = n\left[\alpha I T_2 + I^2R/2 + K(T_m - T_2)\right] \tag{5}$$

where $\alpha = \alpha_P - \alpha_N$ ($\alpha_P$ and $\alpha_N$ are Seebeck coefficients of P- and N-type thermoelectric couple), $I$ is electrical current, $R$ is the electrical resistance of thermoelectric couple, $I^2R$ is Joule heat flux, $K\Delta T$ is Fourier heat leakage rate.

According to FTT, the heat fluxes $Q_H$ and $Q_L$ are:

$$Q_H = K_1(T_H - T_1) \tag{6}$$

$$Q_L = K_2(T_2 - T_0) \tag{7}$$

The energy balance equations of four heat exchange processes are:

$$CGA\eta_{op} - \varepsilon\sigma A\left(T_H^4 - {T_0}^4\right) = K_1(T_H - T_1) \tag{8}$$

$$K_1(T_H - T_1) = m\left[\alpha I T_1 - I^2R/2 + K(T_1 - T_m)\right] \tag{9}$$

$$m\left[\alpha I T_m + I^2R/2 + K(T_1 - T_m)\right] = n\left[\alpha I T_m - I^2R/2 + K(T_m - T_2)\right] \tag{10}$$

$$K_2(T_2 - T_0) = n\left[\alpha I T_2 + I^2R/2 + K(T_m - T_2)\right] \tag{11}$$

where the four junction temperatures ($T_H$, $T_1$, $T_m$ and $T_2$) are unknown. When the sunlight intensity, ambient temperature and structural parameters are fixed, the junction temperatures ($T_H$, $T_1$, $T_m$ and $T_2$) of solar TEG system are fixed, and they can be solved by Eqs. (8)-(11).

This section develops a FTT model of solar-driven two-stage TEG model, and explains its energy conversion processes. This new device can generate electricity by using solar energy and realize waste heat utilization, it has a multi-element structure, so this device has a more practical significance than those models in Refs. (Tayebi et al., 2014; Bellos and Tzivanidis, 2020; Suter et al., 2011; Sun et al., 2022; Montero et al., 2021; Musharavati et al., 2022; Chen, 1996; Eke et al., 2022). Although this model is one-dimensional, the energy conversion processes can be reflected clearly, and performance limits can also be predicted properly. Meanwhile, limited by this one-dimensional structure, the internal heat transfers among thermoelectric modules are fail to be considered. Therefore, a 3D model needs to be established for more accurate performance limits by combining FTT and ANSYS software in future work.

## 3. Main performance parameters

Through above analysis of energy conversion, the output power $P$ and efficiency $\eta$ of system are:

$$P = Q_h - Q_l = m\left[\alpha I(T_1 - T_m) - I^2R\right] + n\left[\alpha I(T_m - T_2) - I^2R\right] \tag{12}$$

$$\eta = P/(CGA) = \left\{m\left[\alpha I(T_1 - T_m) - I^2R\right] + n\left[\alpha I(T_m - T_2) + I^2R\right]\right\}/(CGA) \tag{13}$$

When the total thermoelectric element number $M$ and total heat exchanger inventory $K_T$ are fixed, one can define the heat exchanger inventory ratio $x = K_1/K_T$. Therefore, Eqs. (8)-(11) can be written as:

$$CGA\eta_{op} - \varepsilon\sigma A\left(T_H^4 - {T_0}^4\right) = xK_T(T_H - T_1) \tag{14}$$

$$xK_T(T_H - T_1) = m\left[\alpha I T_1 - I^2R/2 + K(T_1 - T_m)\right] \tag{15}$$

$$m\left[\alpha I T_m + I^2R/2 + K(T_1 - T_m)\right] = (M - m)\left[\alpha I T_m - I^2R/2 + K(T_m - T_2)\right] \tag{16}$$

$$K_T(1 - x)(T_2 - T_0) = (M - m)\left[\alpha I T_2 + I^2R/2 + K(T_m - T_2)\right] \tag{17}$$

Meanwhile, $P$ and $\eta$ can be written as:

$$P = Q_h - Q_l = m\left[\alpha I(T_1 - T_m) - I^2R\right] + (M - m)\left[\alpha I(T_m - T_2) - I^2R\right] \tag{18}$$

$$\eta = P/(CGA) = \left\{m\left[\alpha I(T_1 - T_m) - I^2R\right] + (M - m)\left[\alpha I(T_m - T_2) - I^2R\right]\right\}/(CGA) \tag{19}$$

When the sunlight intensity and structural parameters of the device are given, the temperatures of the receiver and three junctions ($T_H$, $T_1$, $T_m$ and $T_2$) can be determined by equations 14–17. Because Eq. (14) contains quartic terms, the numerical method is applied herein. First, assume the initial junction temperatures ($T_H'$, $T_1'$, $T_m'$ and $T_2'$). Then, solve these temperatures with errors less than $10^{-6}$ by iterative method. Finally, calculate $P$ and $\eta$ by substituting them into Eqs. (18) and (19). The specific computing flow process is shown in Fig. 2.

## 4. Performance analyses and optimizations

In this section, the effects of solar insolation, inner structure parameters and thermal conductance on the optimal performance will be studied. The results will also be compared qualitatively with the experimental results of solar single-stage TEG (Lv et al., 2019, 2021) to verify the validity.

### 4.1. Fixed parameters

The solar TEG device performance characteristics are related to external environment and system structural parameters closely. For actual thermoelectric materials, the physical properties are dynamic as temperature changes (Feng et al., 2018). To simplify the analysis, one can assume that the material properties are fixed, that is, the parameters $\alpha$, $K$ and $R$ are treated as constants in the calculation. The parameters set in this paper is based on the product of IEC1-039018 TEG of Shanghai Jinwei Thermoelectric Co., Ltd. (Chen et al., 2002), and the material used in the device is $Bi_2Te_3$.

Table 1 presents the fixed parameters of solar TEG device.

### 4.2. Junction temperatures under different solar insolation

For different solar insolation $G$, the junction temperatures ($T_H$, $T_1$, $T_m$ and $T_2$) of solar TEG device will change, and the values under different

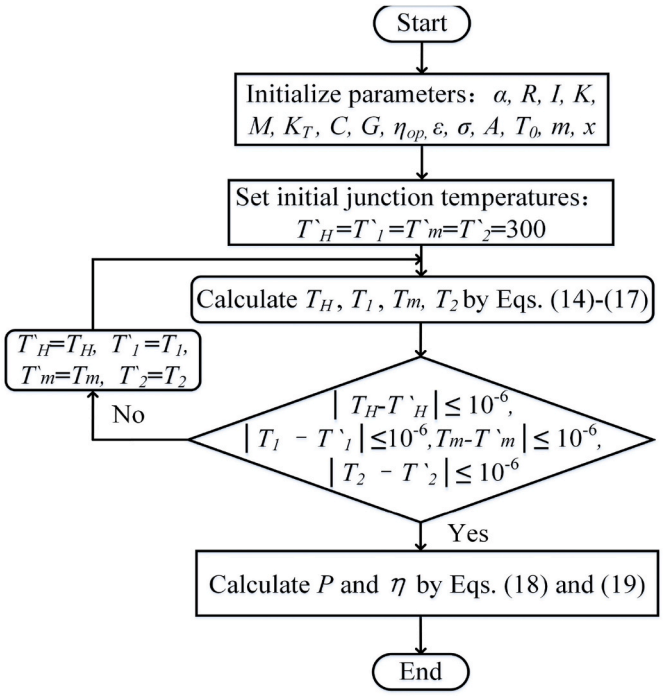


**Fig. 2.** Solving process.

**Table 1**
Fixed parameters of solar TEG device (Chen et al., 2005b; Lai et al., 2019).

| Parameters | Symbol | Value |
|---|---|---|
| Area of receiver | $A$ | $0.07m^2$ |
| Concentration ratio | $C$ | 2000 |
| Solar insolation | $G$ | $1.5W/m^2$ |
| Thermal conductance of thermoelectric element | $K$ | $0.01W/K$ |
| Total heat exchanger inventory | $K_T$ | $10W/K$ |
| Total thermoelectric element number | $M$ | 60 |
| Electrical resistance of thermoelectric element | $R$ | $1.4\times10^{-3}\Omega$ |
| Ambient temperature | $T_0$ | $300K$ |
| Seebeck coefficient | $\alpha$ | $2.3\times10^{-4}V/K$ |
| Optical efficiency | $\eta_{op}$ | 0.95 |
| Emissivity of receiver | $\varepsilon$ | 0.88 |
| Stefan-Boltzmann constant | $\sigma$ | $5.67\times10^{-8}W/(m^2\cdot K^4)$ |

solar insolation $G$ can be solved by combining Eqs. 14–17. Fig. 3 shows the influences of $G$ on junction temperatures. One can see that $T_H$, $T_1$, $T_m$ and $T_2$ increase monotonically versus $G$. It indicates that the operating temperatures increase as solar insolation increases. The junction temperature $T_2$ changes little as $G$ increases, and the working temperature differences $\Delta T_u$ and $\Delta T_l$ of upper and lower TEGs increase versus $G$.

### 4.3. General performance for power output and thermal efficiency

Fig. 4 presents the influences of $I$ and $x$ on $P$ (a) and $\eta$ (b) with $m = 25$. When $I$ is a constant, $P$ and $\eta$ have an extreme value with respect to $x$, respectively. For a fixed $K_T$, $P$ and $\eta$ can be maximized by modulating the inventory allocation rationally. One can find that $P$ and $\eta$ present the same variation trend about $I$ and $x$. The reason is that the heat gain ($CGA$) of solar collector is fixed for fixed sunlight intensity, and the TEG has a fixed heat absorbed rate from the receiver. Therefore, $P$ and $\eta$ show the same variation trend. According to Eqs. (12) and (13), $\eta$ and $P$ are directly proportional ($\eta = P/(CGA_{ab})$), which can also explain this phenomenon. For a fixed $x$, there exists an optimal electrical current $I$ that maximizes $P$ and $\eta$, which is consistent with the results observed in the experiment of solar single-stage TEG (Lv et al., 2019). When $I$ and $x$ are optimal simultaneously, $P$ reaches its maximum value, and corresponding $\eta$ is also maximum. By numerical calculation, the local maximum values of power ($P_{Ix}$) and efficiency ($\eta_{Ix}$) are 7.608 and 0.036, respectively. Compared with solar single-element TEG (Chen, 1996; Eke et al., 2022), this new multi-element device has a larger output power. Benefiting from the two-stage structure, the energy utilization rate is also significantly improved.

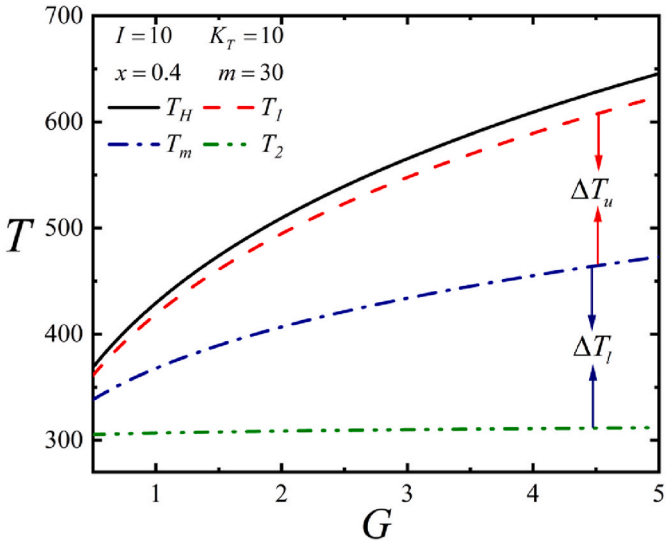


**Fig. 3.** Influences of $G$ on function temperatures.

Fig. 5 presents the $P-m$ (a) and $\eta-m$ (b) curves under different total number $M$. $P$ and $\eta$ exist maximal values about $m$, respectively. It presents that $P$ and $\eta$ can be enhanced by modulating the thermoelectric element allocation suitable for a fixed total thermoelectric element number $M$. One can find that $P$ and $\eta$ show the same variation trend about $m$, and the reason is the same as that in Fig. 4. When $m$ is optimal, $P$ and $\eta$ reach their maximum values $P_m$ and $\eta_m$ simultaneously. Table 2 lists the values of $P_m$ and $\eta_m$ for different thermoelectric element number $M$, and the values of $P_m$ and $\eta_m$ are 7.568 and 0.035 when $M = 60$, respectively. For a fixed $M$, the working temperature difference $T_1 - T_m$ is too small when $m$ is small, and the upper TEG fails to work. Meanwhile, the working temperature difference $T_m - T_2$ is too small when $m$ is too large, and lower TEG fails to work. Therefore, the thermoelectric element numbers $m$ and $n$ should locate in an appropriate range.

For different electrical current $I$, four working temperatures ($T_H$, $T_1$, $T_m$ and $T_2$) can be solved by Eqs. 14–17, and the curves of $P$ and $\eta$ varying with them can be obtained. Fig. 6 shows the relations of $P$ and $\eta$ about four temperatures with $m = 25$ and $x = 0.6$. From above analysis, an optimal electrical current $I_{opt}$ exists to maximize $P$. At this point, the corresponding four working temperatures reach their optimal values ($T_{Hopt}$, $T_{1opt}$, $T_{mopt}$ and $T_{2opt}$), and $T_{Hopt}$ is the optimal collector temperature. One can know from Fig. 6, the maximum power ($P_l$) and efficiency ($\eta_l$) can reach 7.529 and 0.034, respectively. The optimal collector temperature $T_{Hopt} \approx 471K$, and the optimal operating temperatures $T_{1opt} \approx 460K$, $T_{mopt} \approx 365K$ and $T_{2opt} \approx 313K$, respectively.

### 4.4. Optimal performance

Therefore, there exists a group of optimal electrical current, optimal thermoelectric element number $m$ and optimal thermal conductance ratio $x$ to maximize $P$ and $\eta$. The maximum power $P_{max}$ and maximum efficiency $\eta_{max}$ are given by optimizing $I$, $x$ and $m$ simultaneously, and the corresponding efficiency $\eta_P$ and power $P_\eta$ can be further obtained. Since $P$ and $\eta$ reach their maximum values simultaneously, one has $P_{max} = P_\eta$ and $\eta_{max} = \eta_P$.

Fig. 7 gives the curves of $P_{max}$ ($P_\eta$), $\eta_{max}$ ($\eta_P$) and optimal working temperatures versus $T_0$. Table 3 lists $P_{max}$, $\eta_{max}$ and optimal variable

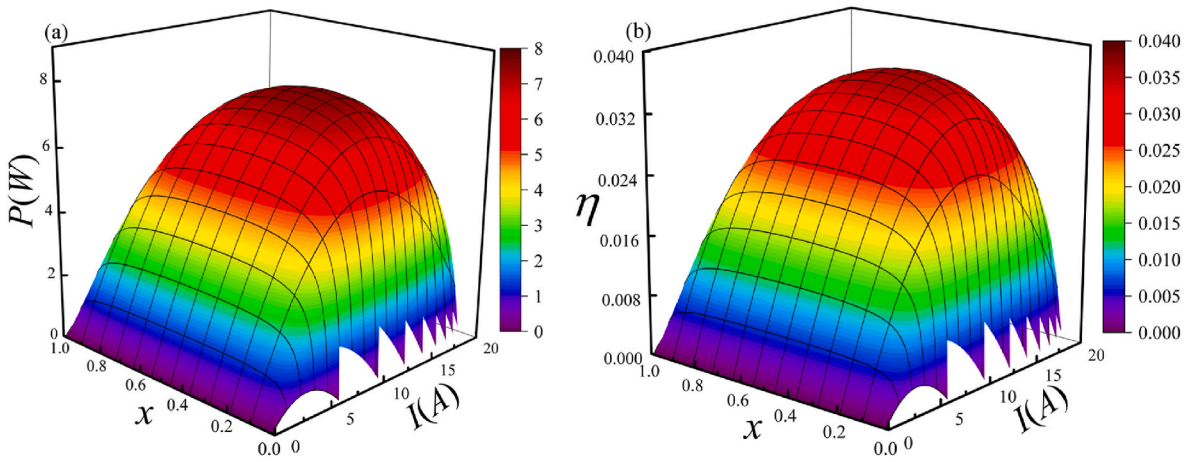


**Fig. 4.** Influences of $I$ and $x$ on $P$ (a) and $\eta$ (b).

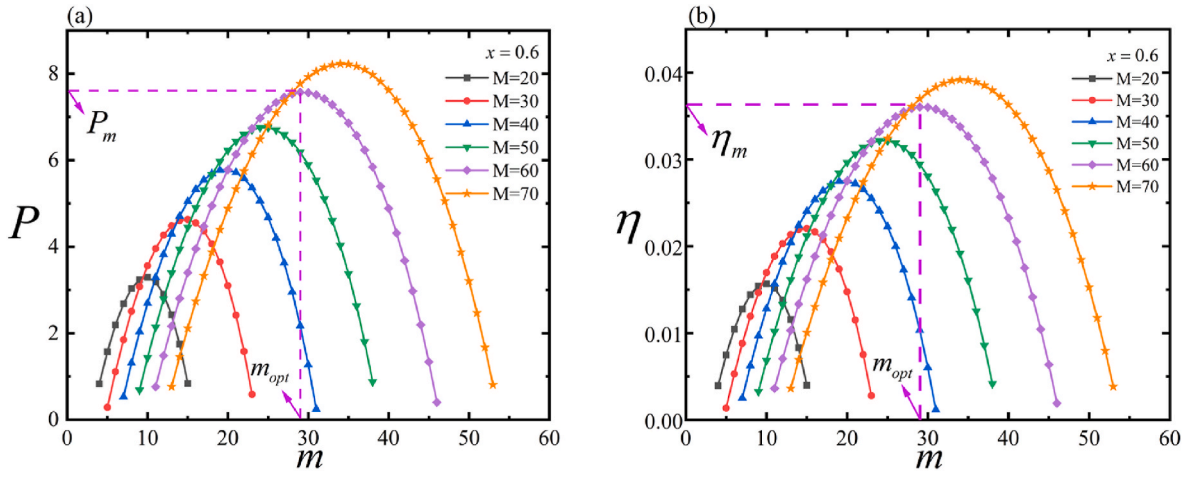


**Fig. 5.** Influences of $m$ on $P$ (a) and $\eta$ (b).

**Table 2**
Values of $P_m$ and $\eta_m$ for different $M$.

| $M$ | 20 | 30 | 40 | 50 | 60 | 70 |
|---|---|---|---|---|---|---|
| $P_m$ | 3.289 | 4.628 | 5.779 | 6.753 | 7.568 | 8.225 |
| $\eta_m$ | 0.015 | 0.022 | 0.027 | 0.032 | 0.034 | 0.039 |

values under different temperatures $T_0$. One can see that the optimal thermoelectric element distribution is close to half, and all of them are 29/60. When the ambient temperature $T_0$ rises, and the operating temperature difference of combined TEG also decreases, so both $P_{max}$ and $\eta_{max}$ decrease, which is the same as the experimental results of solar single-stage TEG (Lv et al., 2019). According to the results in Table 3, $P_{max}$ and $\eta_{max}$ correspond to the same optimal values $x_{opt}$, $m_{opt}$ and $I_{opt}$ for a fixed $T_0$, which is different from the results of two-stage TEG without solar driving (Wu et al., 2021a; Yang et al., 2023). The values of $P_{max}$ and $\eta_{max}$ are 8.14 and 0.039 when $T_0 = 300K$. Compared with the results of $P_{Ix}$ ($\eta_{Ix}$), $P_m$ ($\eta_m$), and $P_I$ ($\eta_I$) in Figs. 4–6, the power after comprehensive optimization is increased by 6.993%, 7.558%, and 8.115%, respectively; and the efficiency is increased by 8.333%, 11.429%, and 12.821%, respectively. When $I$, $x$ and $m$ are optimal, the working temperatures ($T_H$, $T_1$, $T_m$ and $T_2$) of the device also reach their optimal values, respectively. The curve $T_H$ shows the optimal collector temperature. The new performance limits are derived by optimizing external heat transfer processes and internal structural parameters, and they are closer to reality than before.

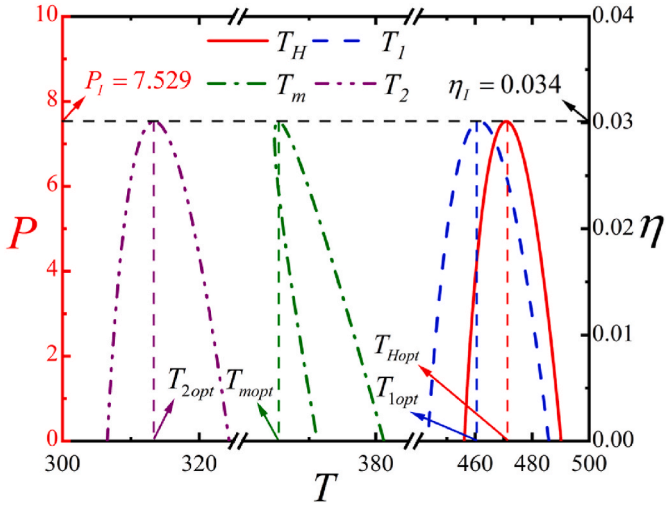


**Fig. 6.** Relations of $P$ and $\eta$ about working temperatures ($T_H$, $T_1$ $T_m$ and $T_2$).

### 4.5. Optimal thermoelectric element allocation with different total numbers

The element number distribution of two-stage TEG at optimal performance is different for different total number $M$. Because $m$ and $n$ are integers, the enumeration method is adopted to study the performance.

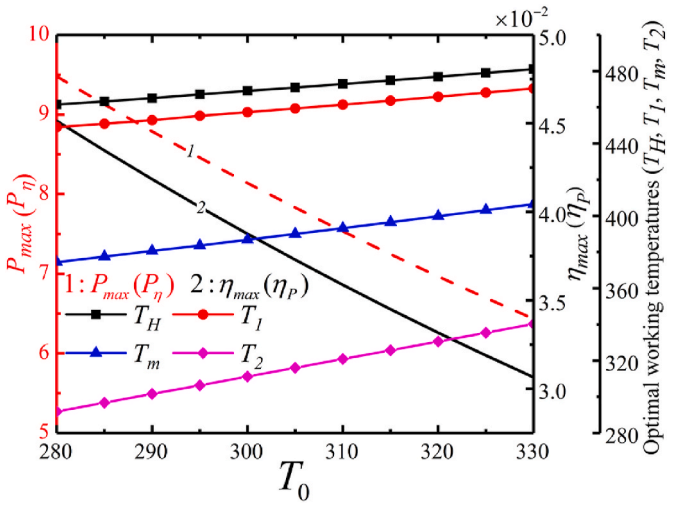


**Fig. 7.** Relations of $P_{max}$ ($P_\eta$), $\eta_{max}$ ($\eta_P$) and optimal working temperatures about $T_0$.

Table 4 presents the optimal thermoelectric element allocation under different $M$. One can know from the table, the thermoelectric element is allocated a half or less than a half to upper TEG, the allocation ratio $m/n$ is same under $P_{max}$ and $\eta_{max}$ objectives. Both $P_{max}$ and $\eta_{max}$ increase as thermoelectric module number $M$ increases, which is the same as the experimental results of solar single-stage TEG (Lv et al., 2019, 2021).

### 4.6. Effects of solar insolation on optimal performance

solar insolation $G$ is a key factor affecting the solar power device performance, $P_{max}$ and $\eta_{max}$ will change when $G$ changes. According to Eqs. 14–19, one can know that the variation law of $P$ and $\eta$ with respect to $G$ is the same as that of concentration ratio $C$. Therefore, only the influences of solar insolation $G$ on $P_{max}$ and $\eta_{max}$ are studied herein. Fig. 8 gives the curves of $P_{max}$ and $\eta_{max}$ about solar insolation $G$. $P_{max}$ and $\eta_{max}$ increase monotonically as solar insolation $G$ increases, and the values of $P_{max}$ and $\eta_{max}$ are 18.319 and 0.044 when $G = 2$. Compared with the optimal performance when $G = 0.75$, $P$ and $\eta$ are increased by 491.92% and 22.22%, respectively. It shows that the solar device performance can be enhanced by improving illumination intensity when structure parameters of system are fixed. The increased amplitude of $\eta_{max}$ become slower gradually as $G$ increases, which is the same as the experimental results of solar single-stage TEG (Lv et al., 2019). The maximal efficiency $\eta_{max}$ converges to 4.5%, it presents the efficiency limit of this model for fixed system structure parameters.

The heat exchanger performance affects the heat flow conversion of system, Fig. 9 depicts the influence of total heat exchanger inventory $K_T$ on $P_{max}$ and $\eta_{max}$. $P_{max}$ and $\eta_{max}$ grow versus $K_T$ monotonically, and they will increase to the upper limits when $K_T$ is large enough, respectively. When the performances of two heat exchangers are improved, the values of power and efficiency can approach $P_{Non-Equil.} = 10.01$ and $\eta_{Non-Equil.} = 0.048$, respectively. When $K_T$ is infinite, the external resistance reduces to zero, and the junction temperatures have $T_1 = T_H$ and $T_2 = T_0$. It becomes a non-equilibrium thermodynamic model. The horizontal lines $P = P_{Non-Equil.}$ and $\eta = \eta_{Non-Equil.}$ in figure show the upper bound of $P$ and $\eta$ for a fixed illumination intensity.

Combining with the relation between $P - I$ and $\eta - I$, the characteristic of $P - \eta$ is depicted in Fig. 10. It is a linear relation between $P$ and $\eta$. This is because the two optimization objectives of $P$ and $\eta$ are consistent, so it presents a linear relation. According to Eq. (13), the slope of line $P - \eta$ is $CGA_{ab}$. When the electric current $I$ is optimal, $P_{max} = 8.141W$ and $\eta_{max} = 0.039$, which corresponds to the optimal values when $T_0 = 300K$ in Table 3.

## 5. Conclusions

A FTT model of solar-driven two-stage multi-element TEG with internal and external irreversible factors is developed. This device can generate electricity by using solar energy, and realizes the cascade uti-

**Table 4**
Optimal thermoelectric element allocation under different $M$.

| $M$ | $m$ | $m/n$ | $P_{max}$ | $\eta_{max}$ |
|---|---|---|---|---|
| 20 | 10 | 10/10 | 4.221 | 0.021 |
| 30 | 14 | 14/16 | 5.615 | 0.027 |
| 40 | 19 | 19/21 | 6.691 | 0.032 |
| 50 | 24 | 24/26 | 7.511 | 0.036 |
| 60 | 29 | 29/31 | 8.14 | 0.039 |
| 70 | 34 | 34/36 | 8.625 | 0.041 |
| 80 | 39 | 39/41 | 8.997 | 0.043 |
| 90 | 44 | 44/46 | 9.281 | 0.044 |
| 100 | 49 | 49/51 | 9.492 | 0.045 |
| 110 | 54 | 54/56 | 9.647 | 0.046 |
| 120 | 58 | 58/62 | 9.758 | 0.047 |
| 130 | 63 | 63/67 | 9.83 | 0.048 |
| 140 | 68 | 68/72 | 9.872 | 0.049 |

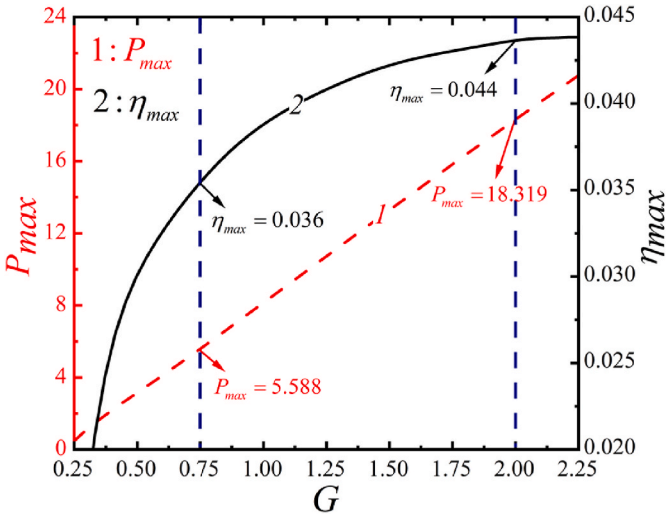


**Fig. 8.** Influence of solar insolation $G$ on $P_{max}$ and $\eta_{max}$ 4.7 Effects of total heat exchanger inventory on optimal performance.

**Table 3**
Values of $P_{max}$, $\eta_{max}$ and optimal variables under different temperatures $T_0$.

| $T_0$ | 285 | 290 | 295 | 300 | 305 | 310 | 315 | 320 | 325 |
|---|---|---|---|---|---|---|---|---|---|
| $x_{opt}$ | 0.5 | 0.5 | 0.5 | 0.5 | 0.5 | 0.5 | 0.5 | 0.5 | 0.5 |
| $m_{opt}$ | 29 | 29 | 29 | 29 | 29 | 29 | 29 | 29 | 29 |
| $n_{opt}$ | 31 | 31 | 31 | 31 | 31 | 31 | 31 | 31 | 31 |
| $I_{opt}$ | 14.411 | 14.154 | 13.641 | 13.385 | 13.123 | 12.872 | 12.615 | 12.359 | 12.103 |
| $P_{max}$ | 9.128 | 8.788 | 8.458 | 8.14 | 7.831 | 7.533 | 7.244 | 6.966 | 6.696 |
| $\eta_{max}$ | 0.043 | 0.041 | 0.041 | 0.039 | 0.037 | 0.036 | 0.034 | 0.033 | 0.032 |

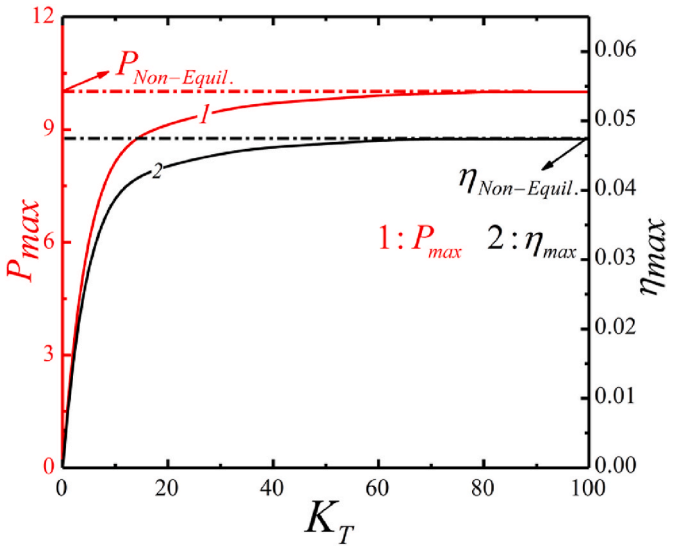


**Fig. 9.** Influence of total thermal conductance $K_T$ on $P_{max}$ and $\eta_{max}$ 4.8 Relation of power versus efficiency.

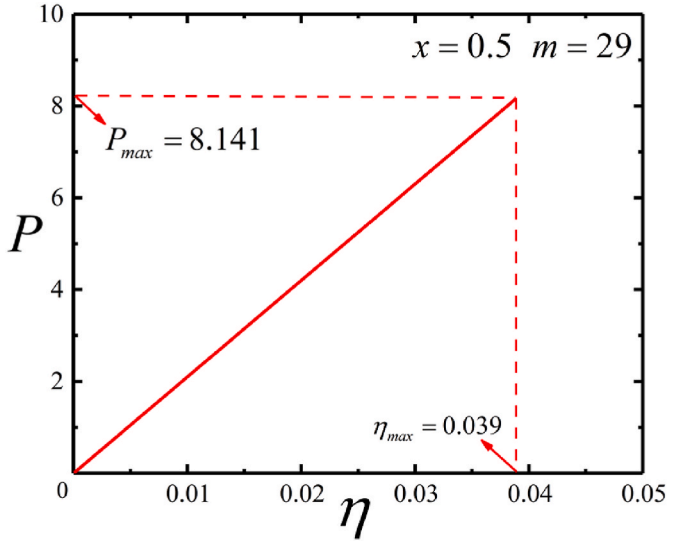


**Fig. 10.** Relation between $P$ and $\eta$.

lization of heat. The working mechanism is explained, power and efficiency are derived and optimized by modulating external heat exchanger inventory and internal structure parameters. The optimal collector temperatures are given, and the effects of external heat transfers, electrical current and solar insolation on optimal performance are also studied. Results show that:

(1) When the structure parameters of device are fixed, an optimal collector temperature exists to maximize power and efficiency, and the two optimization objectives are consistent and show same variation trend. When the power reaches its maximum value, the efficiency also reaches its peak value. Efficiency is proportional to power, and the slope of line $P-\eta$ is $CGA_{ab}$.
(2) When the total heat exchanger inventory and internal structural parameters are fixed, an optimal inventory distribution ratio exists to maximize power and efficiency. When the external heat exchanger parameters are constant, power and efficiency have an extreme value with respect to electrical current and thermoelectric element number $m$, respectively. The thermoelectric element allocation should locate in an appropriate range.
(3) When inventory allocation and internal parameters are optimal simultaneously, the system performance is optimal. At this time, the corresponding receiver and junction temperatures also reach their optimal values, and the optimal heat exchanger inventory ratio is 0.5. The thermoelectric element is allocated a half or less than a half to upper TEG under different total element numbers. Compared to the performances after initial optimization, the power and efficiency are sharply improved after comprehensive optimization.
(4) The external heat transfer resistance will disappear if the total inventory is infinite. In this case, the maximum power and efficiency are the upper bounds for this solar-driven two-stage TEG, and they are the performance limits of non-equilibrium thermodynamic one. When the ambient temperature increases, the system performance will deteriorate. The overall performance can be enhanced by improving the solar insolation.
(5) FTT is an effective tool to optimize the TEG performance. It is necessary to take account into the external heat resistances of TEG device. The performance limits derived by FTT are lower than that of NET, but it can provide more accurate guidance for the optimal design of actual TEG. The results obtained are consistent with the performance characteristics observed in experiments.
(6) Lastly, it has to point out that the one-dimensional model is limited, and the 3D model is needed to be built to explore the system performance deeply by combining FTT and ANSYS software. Moreover, the effects of temperature on the physical property of thermoelectric material should also be considered.

## CRediT authorship contribution statement

**Congzheng Qi:** Conceptualization, Methodology, Software, Writing – original draft. **Yuxuan Du:** Conceptualization, Methodology, Software, Writing – original draft. **Lingen Chen:** Conceptualization, Methodology, Funding acquisition, Supervision, Writing – review & editing. **Yong Yin:** Methodology, Software, Supervision, Validation. **Yanlin Ge:** Methodology, Software, Validation.

## Declaration of competing interest

x The authors declare that they have no known competing financial interests or personal relationships that could have appeared to influence the work reported in this paper.

## Data availability

No data was used for the research described in the article.

## Acknowledgments

This paper is supported by the National Natural Science Foundation of China (Project Nos. 52171317 and 51779262), Graduate Innovative Fund of Wuhan Institute of Technology (Project Nos. CX2022068 and CX2022084) and Science Foundation of Wuhan Institute of Technology (Project No. 19QD22). The authors wish to thank the reviewers for their careful, unbiased and constructive suggestions, which led to this revised manuscript.

## References

Andresen, B., 1983. Finite-Time Thermodynamics. University of Copenhagen, Copenhagen.
Andresen, B., 2011. Current trends in finite-time thermodynamics. Angew. Chem., Int. Ed. 50 (12), 2690–2704.
Andresen, B., Salamon, P., 2022. Future perspectives of finite-time thermodynamics. Entropy 24 (5), 690.

Aranguren, P., Araiz, M., Astrain, D., Martínez, A., 2017. Thermoelectric generators for waste heat harvesting: a computational and experimental approach. Energy Convers. Manag. 148, 680–691.
Bellos, E., Tzivanidis, C., 2020. Energy and financial analysis of a solar driven thermoelectric generator. J. Clean. Prod. 264, 121534.
Berry, R.S., Salamon, P., Andresen, B., 2020. How it all began. Entropy 22 (8), 908.
Cai, H.T., Ye, Z.H., Liu, G.K., Romagnoli, A., Ji, D.X., 2023. Sizing optimization of thermoelectric generator for low-grade thermal energy utilization: module level and system level. Appl. Therm. Eng. 221, 119823.
Chen, J.C., 1996. Thermodynamic analysis of a solar-driven thermoelectric generator. J. Appl. Phys. 79 (5), 2717–2721.
Chen, L.G., Lorenzini, G., 2022. Comparative performance for thermoelectric refrigerators with radiative and Newtonian heat transfer laws. Case Stud. Therm. Eng. 34, 102069.
Chen, L.G., Lorenzini, G., 2023. Heating load, COP and exergetic efficiency optimizations for TEG-TEH combined thermoelectric device with Thomson effect and external heat transfer. Energy 270, 126824.
Chen, L.G., Xia, S.J., 2022a. Heat engine cycle configurations for maximum work output with generalized models of reservoir thermal capacity and heat resistance. J. Non-Equilib. Thermodyn. 47 (4), 329–338.
Chen, L.G., Xia, S.J., 2022b. Maximizing power output of endoreversible non-isothermal chemical engine via linear irreversible thermodynamics. Energy 255, 124526.
Chen, L.G., Xia, S.J., 2022c. Maximizing power of irreversible multistage chemical engine with linear mass transfer law using HJB theory. Energy 261 (Part B), 125277.
Chen, L.G., Xia, S.J., 2023a. Minimum power consumption of multistage irreversible Carnot heat pumps with heat transfer law of $q\propto(\Delta T)^m$. J. Non-Equilib. Thermodyn. 48 (1), 107–118.
Chen, L.G., Xia, S.J., 2023b. Maximum work configuration for irreversible finite-heat-capacity source engines by applying averaged-optimal-control theory. Physica A 617, 128654.
Chen, L.G., Xia, S.J., 2023c. Maximum work configuration of finite potential source endoreversible non-isothermal chemical engines. J. Non-Equilib. Thermodyn. 48 (1), 41–53.
Chen, L.G., Xia, S.J., 2023d. Power-optimization of multistage non-isothermal chemical engine system via Onsager equations, Hamilton-Jacobi-Bellman theory and dynamic programming. Sci. China Technol. Sci. 66 (3), 841–852.
Chen, L.G., Xia, S.J., 2023e. Power output and efficiency optimization of endoreversible non-isothermal chemical engine via Lewis analogy. Sci. China Technol. Sci. 66 https://doi.org/10.1007/s11431-022-2281-8.
Chen, L.G., Wu, C., Sun, F.R., 1999. Finite time thermodynamic optimization or entropy generation minimization of energy systems. J. Non-Equilib. Thermodyn. 22 (4), 327–359.
Chen, L.G., Gong, J.Z., Sun, F.R., Wu, C., 2002. Effect of heat transfer on the performance of thermoelectric generators. Int. J. Therm. Sci. 41 (1), 95–99.
Chen, L.G., Sun, F.R., Wu, C., 2005a. Thermoelectric-generator with linear phenomenological heat-transfer law. Appl. Energy 81 (4), 358–364.
Chen, L.G., Li, J., Sun, F.R., Wu, C., 2005b. Performance optimization of two-stage semiconductor thermoelectric-generators. Appl. Energy 82 (4), 300–312.
Chen, L.G., Meng, F.K., Sun, F.R., 2012. Maximum power and efficiency of an irreversible thermoelectric generator with a generalized heat transfer law. Sci. Iran. 19 (5), 1337–1345.
Chen, L.G., Meng, F.K., Sun, F.R., 2016. Thermodynamic analyses and optimization for thermoelectric devices: the state of the arts. Sci. China Technol. Sci. 59, 442–455.
Chen, L.G., Feng, H.J., Ge, Y.L., 2020a. Maximum energy output chemical pump configuration with an infinite-low- and a finite-high-chemical potential mass reservoirs. Energy Convers. Manag. 223, 113261.
Chen, L.G., Meng, F.K., Ding, Z.M., Xia, S.J., Feng, H.J., 2020b. Thermodynamic modeling and analysis of an air-cooled small space thermoelectric cooler. Eur. Phys. J. Plus 135 (1), 80.
Chen, L.G., Meng, F.K., Ge, Y.L., Feng, H.J., Xia, S.J., 2020c. Performance optimization of a class of combined thermoelectric heating devices. Sci. China Technol. Sci. 63 (12), 2640–2648.
Chen, L.G., Meng, F.K., Ge, Y.L., Feng, H.J., 2021. Performance optimization for a multielement thermoelectric refrigerator with linear phenomenological heat transfer law. J. Non-Equilib. Thermodyn. 46 (2), 149–162.
Chen, W.H., Huang, T.H., Augusto, G.L., Lamba, R., Maduabuchi, C., Saw, L.H., 2022a. Power generation and thermal stress characterization of thermoelectric modules with different unileg couples by recovering vehicle waste heat. J. Clean. Prod. 375, 133987.
Chen, L.G., Qi, C.Z., Ge, Y.L., Feng, H.J., 2022b. Thermal Brownian heat engine with external and internal irreversiblities. Energy 255, 124582.
Chen, L.G., Li, P.L., Xia, S.J., Kong, R., Ge, Y.L., 2022c. Multi-objective optimization of membrane reactor for steam methane reforming heated by molten salt. Sci. China Technol. Sci. 65 (6), 1396–1414.
Chen, L.G., Zhu, F.L., Shi, S.S., Ge, Y.L., Feng, H.J., 2023a. Power and efficiency optimizations of Maisotsenko-Atkinson, Dual and Miller cycles and performance comparisons with corresponding traditional cycles. Sci. China Technol. Sci. 66 https://doi.org/10.1007/s11431-023-2444-1.
Chen, L.G., Shi, S.S., Ge, Y.L., Feng, H.J., 2023b. Performance optimization of a diffusive mass transfer law irreversible isothermal chemical pump. Energy 263 (Part C), 125956.
Chen, L.G., Shi, S.S., Feng, H.J., Ge, Y.L., 2023c. Maximum ecological function performance for a three-reservoir endoreversible chemical pump. J. Non-Equilib. Thermodyn. 48 (2), 179–194.
Chen, L.G., Shi, S.S., Ge, Y.L., Feng, H.J., 2023d. Ecological function performance analysis and multi-objective optimization for an endoreversible four-reservoir chemical pump. Energy (in press).
Cheng, K.L., Qin, J., Jiang, Y.G., Zhang, S.L., Bao, W., 2018. Performance comparison of single-and multi-stage onboard thermoelectric generators and stage number optimization at a large temperature difference. Appl. Therm. Eng. 141, 456–466.
Curzon, F.L., Ahlborn, B., 1975. Efficiency of a Carnot engine at maximum power output. Am. J. Phys. 43 (1), 22–24.
Ebrahimi, Masood, Amin Ahmadi, Mohammad, Khalife, Esmail, 2022. Multi-criteria evaluation, and dynamic modeling of combining thermal photovoltaic and thermoelectric generators to extend electricity generation at night. J. Clean. Prod. 344, 131107.
Eke, M.N., Maduabuchi, C.C., Lamba, R., Njoku, H.O., Ma, X., Gurevich, Y.G., Tyagi, S.K., Ekechukwu, O.V., Ejiogu, E.C., Eneh, C.T., 2022. Exergy analysis and optimization of a two-stage solar thermoelectric generator with tapered legs. Int. J. Exergy 38 (1), 110–136.
Feng, Y.L., Chen, L.G., Meng, F.K., Sun, F.R., 2018. Influences of external heat transfer and Thomson effect on performance of TEG-TEC combined thermoelectric device. Sci. China Technol. Sci. 61 (10), 1600–1610.
Feng, H.J., Wu, Z.X., Chen, L.G., Ge, Y.L., 2021. Constructal thermodynamic optimization for dual-pressure organic Rankine cycle in waste heat utilization system. Energy Convers. Manag. 227, 113585.
Ge, Y.L., Chen, L.G., Feng, H.J., 2021. Ecological optimization of an irreversible Diesel cycle. Eur. Phys. J. Plus 136 (2), 198.
Ge, Y.L., Chen, L.G., Feng, H.J., 2022a. Optimal piston motion configuration for irreversible Otto cycle heat engine with maximum ecological function objective. Energy Rep. 8, 2875–2887.
Ge, Y.L., Shi, S.S., Chen, L.G., Zhang, D.F., Feng, H.J., 2022b. Power density analysis and multi-objective optimization for an irreversible Dual cycle. J. Non-Equilib. Thermodyn. 47 (3), 289–309.
Ge, Y.L., Wu, H., Chen, L.G., Feng, H.J., Xie, Z.H., 2023. Finite time and finite speed thermodynamic optimization for an irreversible Atkinson cycle. Energy 270, 126856.
Ghoreishi, Z., Khalilarya, S., Jafarmadar, S., 2023. The effect of channel dimensions and configuration of thermoelectric elements on the performance of thermoelectric generator module for waste heat recovery. Int. J. Heat Mass Tran. 203, 123787.
Gordon, J.M., 1991. Generalized power versus efficiency characteristics of heat engines: the thermoelectric generator as an illustration. Am. J. Phys. 59 (5), 551–555.
Guo, X.R., Zhang, H.C., Wang, J.T., Zhao, J.P., Wang, F., Miao, H., Yuan, J.L., Hou, S.J., 2020. A new hybrid system composed of high-temperature proton exchange fuel cell and two-stage thermoelectric generator with Thomson effect: energy and exergy analyses. Energy 195, 117000.
He, W., Zhang, G., Zhang, X., Li, J., Li, G.Q., Zhao, X.D., 2015. Recent development and application of thermoelectric generator and cooler. Appl. Energy 143, 1–25.
Hu, C., Fu, T., Liang, T., Chen, X.H., Su, S.H., Chen, J.C., 2021. Efficiency enhancement of an updated solar-driven intermediate band thermoradiative device. Energy 228, 20590.
Jiang, F., Meng, F.K., Chen, L.G., Chen, Z.J., 2022. Thermodynamic analysis and experimental research of water-cooled small space thermoelectric air-conditioner. J. Therm. Sci. 31 (2), 390–406.
Karana, D.R., Sahoo, R.R., 2021. Performance assessment of the automotive heat exchanger with twisted tape for thermoelectric based waste heat recovery. J. Clean. Prod. 283, 124631.
Kong, R., Chen, L.G., Xia, S.J., Li, P.L., Ge, Y.L., 2022. Entropy generation rate minimization for sulfur trioxide decomposition membrane reactor. Energy Rep. 8, 1483–1496.
Lai, X.T., Yu, M.J., Long, R., Liu, Z.C., Liu, W., 2019. Dynamic performance analysis and optimization of dish solar Stirling engine based on a modified theoretical model. Energy 183, 573–583.
Li, J., Chen, L.G., 2022. Optimal configuration of finite source heat engine cycle for maximum output work with complex heat transfer law. J. Non-Equilib. Thermodyn. 47 (4), 433–441.
Li, P.L., Chen, L.G., Xia, S.J., Kong, R., Ge, Y.L., 2022a. Multi-objective optimal configurations of a membrane reactor for steam methane reforming. Energy Rep. 8, 527–538.
Li, P.L., Chen, L.G., Xia, S.J., Kong, R., Ge, Y.L., 2022b. Total entropy generation rate minimization configuration of a membrane reactor of methanol synthesis via carbon dioxide hydrogenation. Sci. China Technol. Sci. 65 (3), 657–678.
Liang, T., Chen, J.Y., Chen, X.H., Su, S.H., Chen, J.C., 2022. Trade-off between the near-field heat transfer and the space charge effect in graphene-anode thermionic energy converters. Energy 260, 125174.
Lin, J., Xie, S., Jiang, C.X., Sun, Y.F., Chen, J.C., Zhao, Y.R., 2022. Maximum power and corresponding efficiency of an irreversible blue heat engine for harnessing waste heat and salinity gradient energy. Sci. China Technol. Sci. 65 (3), 646–656.
Lv, S., He, W., Hu, Z.T., Liu, M.H., Qin, M.H., Shen, S., Gong, W., 2019. High-performance terrestrial solar thermoelectric generators without optical concentration for residential and commercial rooftops. Energy Convers. Manag. 196, 69–76.
Lv, S., Ji, Y.S., Qian, Z.Q., Pan, Y.Y., Zhang, Y.J., He, W., 2021. Preliminary experiment and performance evaluation of a terrestrial solar thermoelectric generators under fluctuant solar radiation. Appl. Therm. Eng. 190, 116753.
Ma, X.L., Zhang, Y.F., Han, Z.H., Zang, N.B., Liu, Z.J., 2023. Performance modelling on a thermoelectric air conditioning system using high power heat sinks and promoting waste heat utilization. Energy 268, 126612.

Meng, F.K., Chen, L.G., Sun, F.R., 2012. Performance characteristics of the multielement thermoelectric generator with radiative heat transfer law. Int. J. Sustain. Energy 31, 119–131.
Meng, F.K., Chen, L.G., Feng, Y.L., Xiong, B., 2017. Thermoelectric generator for industrial gas phase waste heat recovery. Energy 135, 83–90.
Mirhosseini, M., Rezania, A., Rosendahl, L., 2019. Power optimization and economic evaluation of thermoelectric waste heat recovery system around a rotary cement kiln. J. Clean. Prod. 232, 1321–1334.
Montero, F.J., Lamba, R., Ortega, A., Jahn, W., Guzmán, A.M., 2021. A novel 24-h day-night operational solar thermoelectric generator using phase change materials. J. Clean. Prod. 296, 126553.
Musharavati, F., Khanmohammadi, S., Nondy, J., Gogoi, T.K., 2022. Proposal of a new low-temperature thermodynamic cycle: 3E analysis and optimization of a solar pond integrated with fuel cell and thermoelectric generator. J. Clean. Prod. 331, 129908.
Patil, D.S., Arakerimath, R.R., Walke, P.V., 2018. Thermoelectric materials and heat exchangers for power generation-a review. Renew. Sustain. Energy Rev. 95, 1–22.
Paul, R., Hoffmann, K.H., 2022. Optimizing the piston paths of Stirling cycle cryocoolers. J. Non-Equilibr. Thermodyn. 47 (2), 195–203.
Pourkiaei, S.M., Ahmadi, M.H., Sadeghzadeh, M., Moosavi, S., Pourfayaz, F., Chen, L.G., Yazdi, M.A., Kumar, R., 2019. Thermoelectric cooler and thermoelectric generator devices: a review of present and potential applications, modeling and materials. Energy 186, 115849.
Prajapati, P., Patel, V., Raja, B.D., Jouhara, H., 2023. Multi objective ecological optimization of an irreversible Stirling cryogenic refrigerator cycle. Energy 274, 127253.
Qi, C.Z., Ding, Z.M., Chen, L.G., Ge, Y.L., Feng, H.J., 2021. Modelling of irreversible two-stage combined thermal Brownian refrigerators and their optimal performance. J. Non-Equilib. Thermodyn. 46 (2), 175–189.
Qiu, S.S., Ding, Z.M., Chen, L.G., Ge, Y.L., 2021a. Performance optimization of thermionic refrigerators based on van der Waals heterostructures. Sci. China Technol. Sci. 64 (5), 1007–1016.
Qiu, S.S., Ding, Z.M., Chen, L.G., Ge, Y.L., 2021b. Performance optimization of three-terminal energy selective electron generators. Sci. China Technol. Sci. 64 (8), 1641–1652.
Qiu, S.S., Chen, L.G., Ding, Z.M., Ge, Y.L., 2022. Performance optimization of a solar-driven single-stage heterostructure-based thermionic generator. Sci. Sin. Tech. 52 (12), 1901–1911 (in Chinese).
Ranjbar, B., Mehrpooya, M., Marefati, M., 2021. Parametric design and performance evaluation of a novel solar assisted thermionic generator and thermoelectric device hybrid system. Renew. Energy 164, 194–210.
Selimefendigil, F., Öztop, H.F., 2020. Performance assessment of a thermoelectric module by using rotating circular cylinders and nanofluids in the channel flow for renewable energy applications. J. Clean. Prod. 279, 123426.
Shittu, S., Li, G.Q., Zhao, X.D., Ma, X.L., 2020. Review of thermoelectric geometry and structure optimization for performance enhancement. Appl. Energy 268, 115075.
Sieniutycz, S., 2020. Complexity and Complex Thermo-Economic Systems. Elsevier.
Sun, Z.Y., Luo, D., Wang, R.C., Li, Y., Yan, Y.Y., Cheng, Z.M., Chen, J., 2022. Evaluation of energy recovery potential of solar thermoelectric generators using a three-dimensional transient numerical model. Energy 256, 124667.
Suter, C., Tomes, P., Weidenkaff, A., Steinfeld, A., 2011. A solar cavity-receiver packed with an array of thermoelectric converter modules. Sol. Energy 85 (7), 1511–1518.
Tayebi, L., Zamanipour, Z., Vashaee, D., 2014. Design optimization of micro-fabricated thermoelectric devices for solar power generation. Renew. Energy 69 (3), 166–173.
Tian, L., Chen, L.G., Ren, T.T., Ge, Y.L., Feng, H.J., 2022a. Optimal distribution of heat exchanger area for maximum efficient power of thermoelectric generators. Energy Rep. 8, 10492–10500.
Tian, L., Chen, L.G., Ge, Y.L., Shi, S.S., 2022b. Maximum efficient power performance analysis and multi-objective optimization of two-stage thermoelectric generators. Entropy 24 (10), 1443.
Tohidi, F., Holagh, S.G., Chitsaz, A., 2022. Thermoelectric generators: a comprehensive review of characteristics and applications. Appl. Therm. Eng. 201, 117793.
Tyagi, K., Gahtori, B., Kumar, S., Dhakate, S., 2023. Advances in solar thermoelectric and photovoltaic-thermoelectric hybrid systems for power generation. Sol. Energy 254, 195–212.
Wu, Z.X., Feng, H.J., Chen, L.G., Tang, W., Shi, J.Z., Ge, Y.L., 2020. Constructal thermodynamic optimization for ocean thermal energy conversion system with dual-pressure organic Rankine cycle. Energy Convers. Manag. 210, 112727.
Wu, Z.X., Chen, L.G., Feng, H.J., Ge, Y.L., 2021a. Constructal thermodynamic optimization for a novel Kalina-organic Rankine combined cycle to utilize waste heat. Energy Rep. 7, 6095–6106.
Wu, H., Ge, Y.L., Chen, L.G., Feng, H.J., 2021b. Power, efficiency, ecological function and ecological coefficient of performance optimizations of an irreversible Diesel cycle based on finite piston speed. Energy 216, 119235.
Xiong, B., Chen, L.G., Meng, F.K., Sun, F.R., 2014. Modeling and performance analysis of a two-stage thermoelectric energy harvesting system from blast furnace slag water waste heat. Energy 77, 562–569.
Xiong, B., Chen, L.G., Meng, F.K., Sun, F.R., 2016. Thermodynamic analysis and optimization for a two-stage thermoelectric generator device with cylindrical tubes driven by sintering flue gas heat. Sci. Sin. Tech. 46 (3), 293–301 (in Chinese).
Xiong, Q.G., Hajjar, A., Alshuraiaan, B., Izadi, M., Altnji, S., Shehzad, S.A., 2021. State-of-the-art review of nanofluids in solar collectors: a review based on the type of the dispersed nanoparticles. J. Clean. Prod. 310, 127528.
Xu, H.R., Chen, L.G., Ge, Y.L., Feng, H.J., 2022. Multi-objective optimization of Stirling heat engine with various heat transfer and mechanical losses. Energy 256, 124699.
Yang, W.H., Feng, H.J., Chen, L.G., Ge, Y.L., 2023. Power and efficiency optimizations of a simple irreversible supercritical organic Rankine cycle. Energy 278, 127755.
Yuan, D.D., Jiang, W., Xiao, J.J., Ling, X.W., Zhang, Y.F., Lu, R., 2023. Experimental study on the temperature-regulating function of road thermoelectric generator system. J. Clean. Prod. 384, 135586.
Zang, P.C., Ge, Y.L., Chen, L.G., Gong, Q.R., 2022. Power density characteristic analysis and multi-objective optimization of an irreversible porous medium engine cycle. Case Stud. Therm. Eng. 35, 102154.
Zhang, H.C., Xu, H.R., Chen, B., Dong, F.F., Ni, M., 2017. Two-stage thermoelectric generators for waste heat recovery from solid oxide fuel cells. Energy 132, 280–288.
Zhang, X., Yang, G.F., Yan, M.Q., Ang, L.K., Ang, Y.S., Chen, J.C., 2021. Design of an all-day electrical power generator based on thermoradiative devices. Sci. China Technol. Sci. 64 (10), 2166–2173.
Zhao, Y.L., Lu, M.J., Li, Y.Z., Wang, Y.L., Ge, M.H., 2023. Numerical investigation of an exhaust thermoelectric generator with a perforated plate. Energy 263, 125776.
Zhu, W.C., Xu, A.Q., Yang, W.L., Xiong, B.Y., Xie, C.J., Li, Y., Xu, L.M., Shi, Y., Lin, W., 2022. Optimal design of annular thermoelectric generator with twisted tape for performance enhancement. Energy Convers. Manag. 270, 116258.